iScience

CellPress
OPEN ACCESS

Article

Sirtuin 2 regulates neutrophil functions through NAD^+ synthesis pathway in virus infection

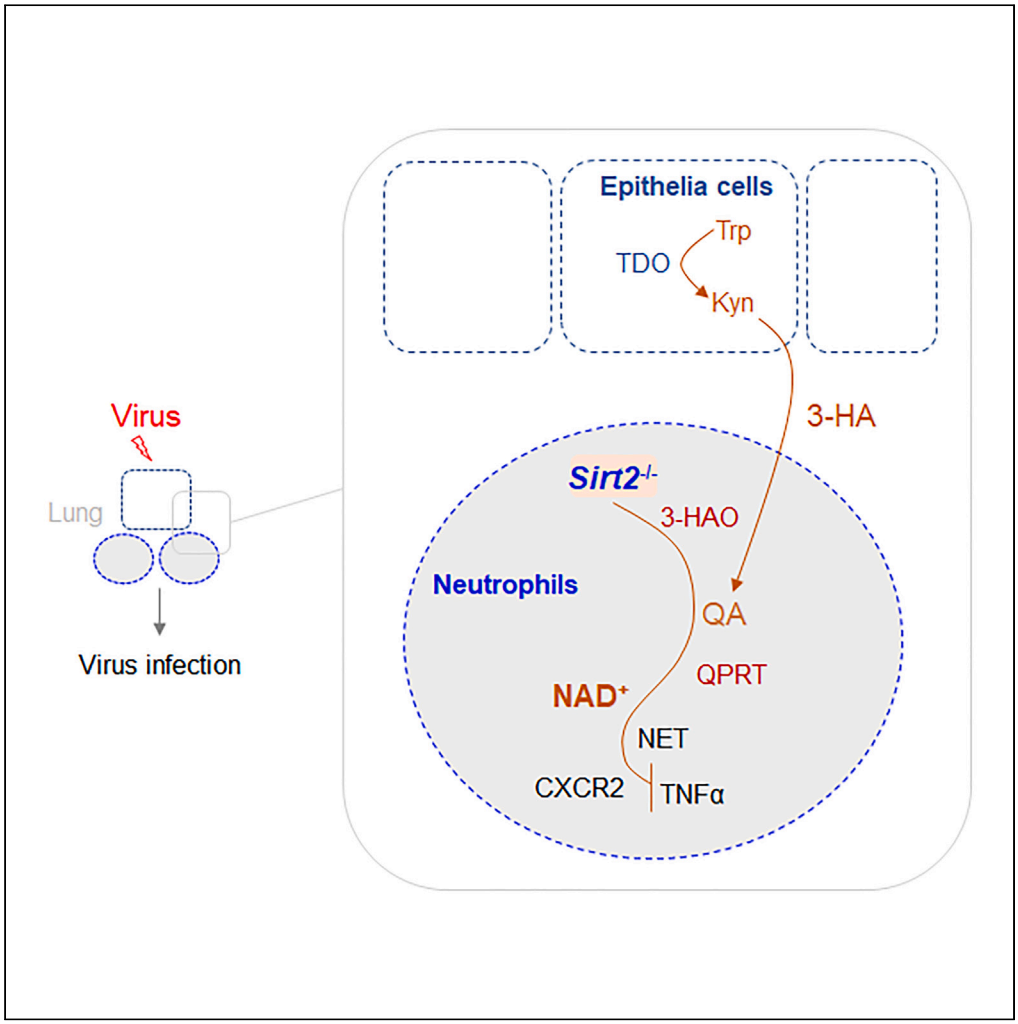

Zhiyuan Zhang, Qiuli Yang, Yingjie Dong, ..., Jingxuan Xia, Yujing Bi, Guangwei Liu

byj7801@sina.com (Y.B.)
liugw@bnu.edu.cn (G.L.)

Highlights

SIRT2 regulates the functions of neutrophils in virus infection

Endogenous quinolinic acid is critical for neutrophil function induced by *Sirt2*$^{-/-}$

SIRT2 downregulates 3-HAO and QPRT to use quinolinic acid for NAD^+ synthesis

Epithelial cells-derived 3-HA is a source of intracellular quinolinic acid in neutrophils

Zhang et al., iScience *27*, 110184
July 19, 2024
https://doi.org/10.1016/j.isci.2024.110184

iScience

CellPress
OPEN ACCESS

Article

Sirtuin 2 regulates neutrophil functions through NAD^+ synthesis pathway in virus infection

Zhiyuan Zhang,[1,3] Qiuli Yang,[1,3] Yingjie Dong,[1,3] Likun Wang,[2,3] Ruiying Niu,[1] Jingxuan Xia,[1] Yujing Bi,[2,*] and Guangwei Liu[1,4,*]

SUMMARY

Neutrophils play an important role in antiviral immunity, but the underlying mechanisms remain unclear. Here, we found that SIRT2 deficiency inhibited the infiltration of neutrophils, as well as the secretion of inflammatory cytokines and the formation of neutrophil extracellular traps (NETs), ameliorating disease symptoms during acute respiratory virus infection. Mechanistically, SIRT2 deficiency upregulates quinolinic acid (QA)-producing enzyme 3-hydroxyanthranilate oxygenase (3-HAO) and leads to expression of quinolinate phosphoribosyltransferase (QPRT), which promotes the synthesis of QA for NAD^+ and limits viral infection when *de novo* NAD^+ synthesis is blocked. Tryptophan-2,3-oxygenase expressed in epithelial cells metabolizes tryptophan to produce kynurenine and 3-hydroxyaminobenzoic acid, which is a source of intracellular QA in neutrophils. Thus, our findings reveal a previously unrecognized QPRT-mediated switch in NAD^+ metabolism by exploiting neutrophil-derived QA as an alternative source of replenishing intracellular NAD^+ pools induced by SIRT2 to regulate neutrophil functions during virus infection, with implications for future immunotherapy approaches.

INTRODUCTION

The tryptophan (Trp) metabolism pathway plays key roles in various physiological and pathological processes.[1–3] Trp metabolites have received extensive attention for their roles in immune regulation, especially immunosuppression in cancer, graft survival, aging, and neurodegenerative diseases.[4–7] A previous study showed that ginseng polysaccharides increase the antitumor response to αPD-1 mAb by decreasing the L-kynurenine concentration and the Kyn/Trp ratio, which contributes to the suppression of regulatory T cells.[8] Aryl hydrocarbon receptor (AHR) activation by tryptophan (Trp) catabolites enhances tumor malignancy and suppresses antitumor immunity.[4] Quinolinic acid (QA) is a product of tryptophan degradation and a universal *de novo* precursor of nicotinamide adenine dinucleotide (NAD^+), an important enzymatic cofactor for enzymes that supports the generation of cellular energy, maintenance of cell survival, delay of cell aging, and regulation of immune activity.[9–11] QA accumulates in neurodegenerative disorders, including Alzheimer's disease and Huntington's disease, where it is thought to be toxic to neurons.[11] Gliomas decompose and metabolize tryptophan, especially by producing QA, which affects tumor progression.[12] The Trp-to-QA pathway has been shown to be critical in several psychiatric conditions, such as depression and stress-related disorders.[13] QA directs a portion of Trp catabolism toward replenishing NAD^+ levels in response to inflammation.[14] However, the roles of the tryptophan metabolite QA and the QA-NAD^+ pathway in preventing viral infection in neutrophils have not been determined.

Sirtuins are NAD^+-dependent class III histone deacetylases that are emerging as crucial regulators of T cell-mediated adaptive immunity.[15] Sirtuin 2 (SIRT2) is a cytosolic enzyme that is known to shuttle to the nucleus during mitosis and certain bacterial infections.[16] They play a considerable role in critical cellular processes such as cellular metabolism, cellular homeostasis, tumor suppression, and inflammation.[17–19] Although it has been proposed that SIRT2 has a central role in some diseases, its specific function remains controversial. However, whether SIRT2 has a regulatory effect on the antiviral infection ability of neutrophils and its underlying mechanism are unclear.

Herein, we showed that the NAD^+-dependent metabolic sensor SIRT2 regulates neutrophil function in preventing viral infection. The endogenous tryptophan metabolite and NAD^+ precursor QA are critical for the neutrophil function induced by SIRT2. SIRT2 deficiency upregulates the QA-producing enzyme 3-hydroxyanthranilate oxygenase (3-HAO) and leads to the expression of quinolinate phosphoribosyltransferase (QPRT), which promotes the synthesis of NAD^+ and limits viral infection when *de novo* NAD^+ synthesis is blocked. This provides a QPRT-mediated switch in NAD^+ metabolism by exploiting neutrophil-derived QA as an alternative source of replenishing intracellular NAD^+ pools to regulate neutrophil functions during virus infection.

[1]Key Laboratory of Cell Proliferation and Regulation Biology, Ministry of Education, College of Life Sciences, Beijing Normal University, Beijing 100875, China
[2]State Key Laboratory of Pathogen and Biosecurity, Academy of Military Medical Science, Beijing 100071, China
[3]These authors contributed equally
[4]Lead contact
*Correspondence: byj7801@sina.com (Y.B.), liugw@bnu.edu.cn (G.L.)
https://doi.org/10.1016/j.isci.2024.110184

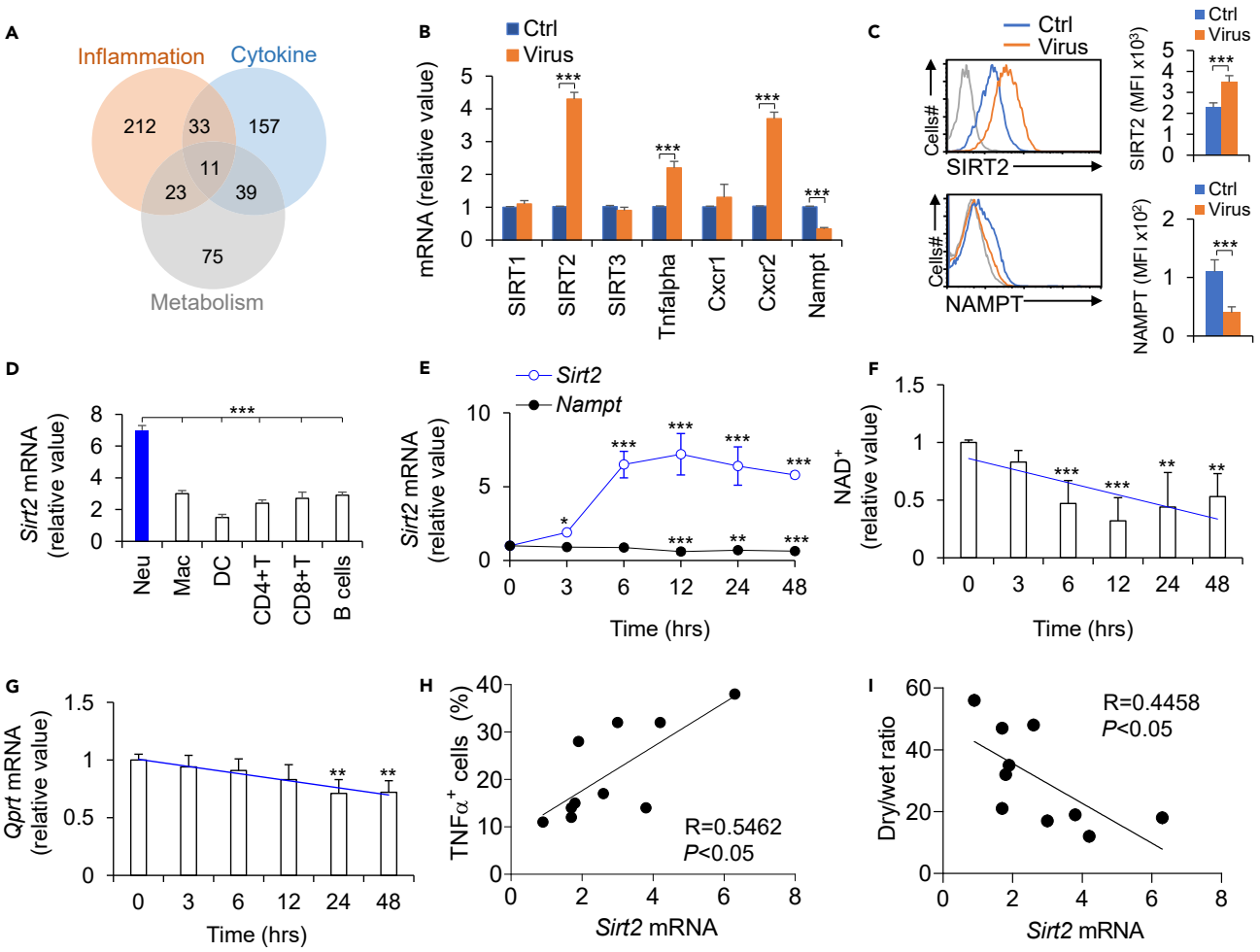

Figure 1. SIRT2 expression is associated with NAD⁺ synthesis and neutrophil function during virus infection

(A) C57BL/6 mice were infected with or without the PR8 virus for 48 h, after which the lungs were collected. RNA was analyzed via microarray analysis to compare the expression profiles of control and virus-infected cells from the lung with those of certain genes involved in surface and intracellular signaling pathways.

(B) The expression of the indicated molecules was examined via qPCR analyses of neutrophils in BALF from PBS (ctrl)-treated or virus-infected mice (the expression in the control groups was set to 1).

(C) Expressions of SIRT2 and NAMPT in neutrophils in BALF from PBS (ctrl)- or virus (virus)-infected mice by flow cytometry.

(D) *Sirt2* mRNA expression was examined by qPCR analyses in the indicated cell populations isolated from BALF from virus-infected mice.

(E) *Sirt2* and *Nampt* mRNA expression in neutrophils isolated from BALF was examined via qPCR at different time points following virus infection in mice.

(F and G) Changes in the NAD^+ (F) and *Qprt* mRNA levels (G) in neutrophils isolated from BALF at different time points following virus infection.

(H and I) The correlation between the percent of TNF-α^+ cells among neutrophils (H) or the dry/wet weight ratio of the lung (I) and the expression of *Sirt2* in neutrophils during virus infection. The data are representative of three or four independent experiments (n = 4–10 mice per group). $^{**}p < 0.01$ and $^{***}p < 0.001$, compared with the indicated groups.

RESULTS

SIRT2 expression and NAD^+ levels are related to neutrophil function in antiviral infection

We first analyzed the gene expression profiles of neutrophils from bronchoalveolar lavage fluid (BALF) from vehicle and virus-infected mice using Affymetrix oligonucleotide arrays and found that the expression of select groups of surface and intracellular inflammatory signaling molecules, including those related to inflammation, cytokines, and metabolism, as described in Figure 1A, was altered in virus-infected neutrophils compared with uninfected neutrophils. Virus-infected neutrophils exhibited upregulated SIRT2 expression. The expression of SIRT2, Tnf-α, and Cxcr2 in the neutrophils from the BALF of virus-infected mice was significantly upregulated, but the expression of nicotinamide phosphoribosyltransferase (NAMPT) was significantly downregulated (Figures 1B and 1C), which suggested that these molecules, including the NAD^+-dependent deacetylase SIRT2 and the NAD^+ synthetic pathway rate-limiting enzyme NAMPT, are likely involved in regulating the functions of neutrophils infected by viruses.

Furthermore, we found that SIRT2 expression was significantly increased in infiltrating neutrophils but not in macrophages, dendritic cells (DCs), B cells, or T cells in BALF after virus infection (Figure 1D). Subsequently, the relationship between SIRT2 and NAD^+ synthetic pathways was studied. NAMPT is the rate-limiting enzyme which catalyzes the conversion of nicotinamide (NAM), nicotinic acid (NA), and phosphoribosyl-pyrophosphates to nicotinamide mononucleotide (NMN) in the mammalian NAD^+ synthetic salvage pathway. It found that SIRT2 expression was continuously upregulated, while NAD^+ levels, NAMPT, and QPRT were continuously downregulated in a time-course-dependent manner (Figures 1E-1G). Additionally, the expression of SIRT2 in neutrophils infiltrated by viral infection was positively correlated with the secretion of the proinflammatory factor TNF-α but negatively correlated with the dry/wet weight ratio of the lungs (Figures 1H and 1I). Taken together, these data suggest that the SIRT2 and NAD^+ synthesis pathways, including the salvage pathway (NAMPT) and *de novo* pathway (QPRT), are likely involved in regulating neutrophil function during antiviral infection.

SIRT2 deficiency limits neutrophil infiltration and functions in ameliorating viral infection-related inflammation

To ascertain the role of SIRT2 in neutrophils during virus infection, we generated myeloid-specific SIRT2 conditional knockout mice with *Sirt2*$^{flox/flox}$ mice and *lyz-cre* mice, and these mice are referred to as *Sirt2*$^{-/-}$ mice hereafter. We found that the disease clinical score, dry and wet weight ratio of the lung, and inflammatory cell infiltration worsened after virus infection in wild-type (WT) mice. However, SIRT2 deficiency alleviated these alterations (Figures 2A–2D). Although *Sirt2*$^{-/-}$ did not alter the percentage of $CD44^{high}CD62^{low}CD4^+$T cells or $CD44^{high}CD62L^{low}CD8^+$ T cells (Figures S1A and S1B), it resulted in decreased infiltration of neutrophils in the BALF and lung (Figures 2E and S2A), as well as the production of the proinflammatory cytokine TNF-α in neutrophils (Figures 2F and S2B).

It has been shown that neutrophil extracellular traps (NETs) are crucial for the function of neutrophils.[20,21] NETs are composed of extracellular DNA (exDNA) and histone and nonhistone proteins that regulate NET formation and antimicrobial activities.[22,23] We then observed changes in neutrophil NETs in mice infected with the virus. The results showed that the percent of neutrophil NETs and the expression of citrulline histone H3 (cit-H3) were increased after virus infection. However, the absence of SIRT2 significantly inhibited these changes (Figures 2G–2I, S3A, and S3B). These findings suggest that SIRT2 is crucial for inducing neutrophil NET formation during virus infection in mice. Altogether, these data collectively reveal that SIRT2 regulates the infiltration and function of neutrophils in viral infection-related inflammation.

CXCR2 is critically involved in regulating neutrophil function induced by *Sirt2*$^{-/-}$ during virus infection

CXCR2 is critical for regulating NET formation in neutrophils during inflammation.[8] We first checked CXCR2 surface expression in neutrophils during virus infection. The percent and MFI of CXCR2 were enhanced in neutrophils in BALF, blood, and spleen after virus infection (Figures 3A, 3B, S4A, and S4B). Furthermore, although the absence of SIRT2 alleviated the clinical score of the disease (Figure 3C) and the dry/wet weight ratio of the lungs (Figure 3D), the percent of neutrophil infiltration (Figures 3E and 3F), the production of the proinflammatory factor TNF-α (Figures 3G and 3H), the percent of NETs (Figure 3I) and the level of CitH3 expression (Figure 3J) in neutrophils during virus infection and the blockade of CXCR2 expression with CXCR2 inhibitor treatment significantly attenuated these changes. These findings suggest that CXCR2 is crucial for the NET formation and functional activities of neutrophils induced by *Sirt2*$^{-/-}$ in mice during virus infection.

QA constitutes a NAD^+ salvage pathway involved in regulating neutrophil function induced by *Sirt2*$^{-/-}$

As reported[9–11] and previously shown, the NAD^+ level and the NAD^+ synthesis pathway are important for the activity of the NAD^+-dependent deacetylase SIRT2. We then examined the effects of SIRT2 deficiency on NAD^+ pathway signaling in neutrophils challenged with viruses (Figure 4A). Neutrophils isolated from mouse spleens were stimulated with viruses, and the results showed that SIRT2 deficiency upregulated NAD^+ levels (Figure 4B). Moreover, SIRT2 deficiency led to decreased metabolite QA and increased NMN but not NA or NAM in neutrophils stimulated with viruses (Figure 4C). These data reveal that the NAD^+ level and the NAD^+ synthesis pathway is likely involved in the regulation of neutrophil function induced by *Sirt2*$^{-/-}$.

As QA may serve as a precursor for NAD^+, which in turn may direct a portion of Trp catabolism toward replenishing NAD^+ levels in response to inflammation, we next assessed the functional consequences of QA for NAD^+-mediated immune responses in neutrophils induced by *Sirt2*$^{-/-}$ during antiviral infection. Blocking *de novo* NAD^+ synthesis with the NAMPT inhibitor FK866 significantly reduced NAD^+ levels in neutrophils and enhanced TNF-α production, NET formation, and citH3 and CXCR2 expression in neutrophils induced by *Sirt2*$^{-/-}$ (Figures 4D–4H), which indicated that neutrophil functional activities require NAMPT-mediated NAD^+ synthesis for antiviral infection. QA, but not NA, restored NAD^+ levels, the production of TNF-α, NET formation, and the expression of citH3 and CXCR2 via NAMPT inhibition in neutrophils (Figures 4D–4H), indicating that neutrophils use QA to replenish NAD^+ stocks and regulate the neutrophil function induced by *Sirt2*$^{-/-}$ during virus infection. These data reveal that the QA-fed but not the NA-fed NAD^+ salvage pathway is activated in *Sirt2*$^{-/-}$ neutrophils during virus infection. Collectively, these data suggest that the functional activities of neutrophils in preventing viral infection are associated with a switch from the NA salvage pathway to the QA salvage pathway to synthesize NAD^+ to regulate the functions of neutrophils induced by SIRT2.

QPRT is expressed in neutrophils and is responsible for NAD^+ synthesis induced by *Sirt2*$^{-/-}$

To identify the QA-mediated NAD^+ synthesis pathway involved in the regulation of neutrophil functions induced by *Sirt2*$^{-/-}$ in the context of antiviral infection, we analyzed the expression of QPRT, the enzyme that is responsible for the generation of NAD^+ from QA. SIRT2 deficiency

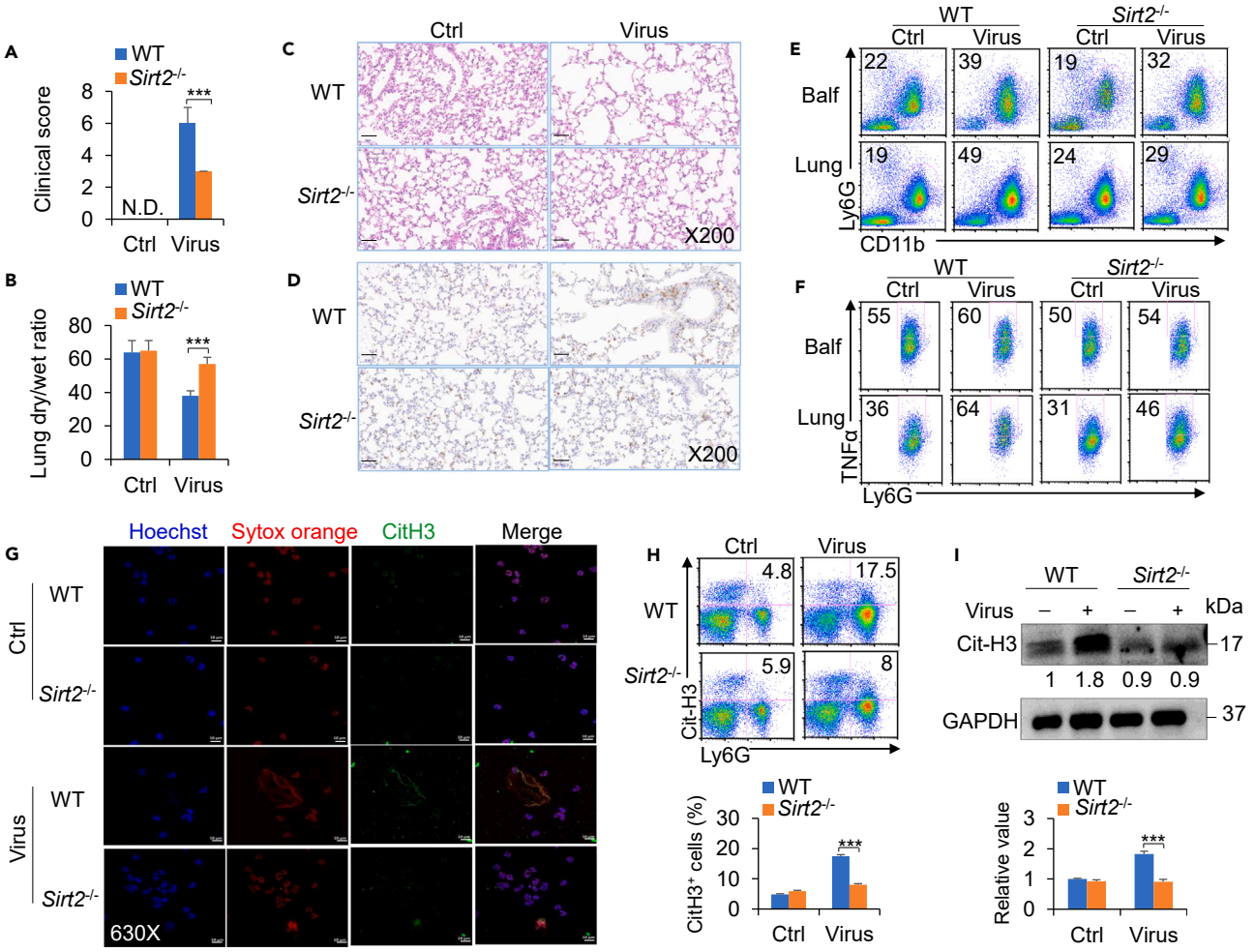

Figure 2. SIRT2 deficiency limits neutrophil infiltration and function in ameliorating viral infection-related inflammation

WT and *Sirt2*$^{-/-}$ mice were challenged with PBS (ctrl) or subjected to PR8 virus infection for 48 h. Clinical score of infected mice (A) and the ratio of dry and wet weights of lungs (B) from mice.

(C) Hematoxylin and eosin (H&E) staining of mouse lungs at 48 h after challenge with PBS or the PR8 virus.

(D) Immunohistochemical staining of anti-Ly6G in the lungs at 48 h after challenge with PBS or the PR8 virus.

(E) Flow cytometry analysis of CD11b^{+}Ly6G^{+} cells in the bronchoalveolar lavage fluid (BALF) or lungs of WT and *Sirt2*$^{-/-}$ mice challenged with PBS (ctrl) or PR8 virus infection for 48 h. Dot plots present representative flow cytometry data.

(F) Intracellular staining of TNF-α in CD11b^{+}Ly6G^{+} cells in the BALF or lungs of WT and *Sirt2*$^{-/-}$ mice challenged with PBS (ctrl) or PR8 virus infection for 48 h. Dot plots present representative flow cytometry data.

(G) NETs from CD11b^{+}Ly6G^{+} neutrophils were isolated from BALF from WT and *Sirt2*$^{-/-}$ mice at 48 h after PR8 infection. Typical NET images are displayed. Scale bars, 10 μm; original magnification, 630×.

(H) Intracellular staining of CitH3 in Ly6G^{+} cells in BALF from WT and *Sirt2*$^{-/-}$ mice at 48 h after PR8 infection. Dot plots present representative flow cytometry data (upper panel), and the statistical results are shown (lower panel).

(I) Western blot analysis of the CitH3 in Ly6G^{+} cells sorted from BALF from WT and *Sirt2*$^{-/-}$ mice 48 h after challenge with PBS (ctrl) or PR8 infection. The data are representative of three or four independent experiments (n = 3–6 mice per group). ***$p < 0.001$, compared with the indicated groups.

led to significant upregulation of QPRT and 3-HAO expression in BALF-infiltrated neutrophils from virus-infected mice (Figures 5A–5D). Additionally, different toll-like receptor (TLR) ligands can stimulate neutrophils, and similar expression of QPRT was induced by *Sirt2*$^{-/-}$ (Figure 5C). These results indicate that QPRT and 3-HAO are likely involved in regulating the NAD^{+} synthesis induced by *Sirt2*$^{-/-}$ through QPRT.

To test the role of QPRT in regulating the NAD^{+} synthesis and neutrophil function induced by *Sirt2*$^{-/-}$, we knocked down *Qprt* with shRNA (Figure S5). SIRT2 deficiency in combination with control shRNA increased the level of NAD^{+} and recruited more neutrophils and upregulated the production of TNF-α in neutrophils challenged with virus, but SIRT2 deficiency combined with Qprt shRNA significantly restored these changes to the control level (Figures 5E–5H). These data suggest that QPRT-mediated NAD^{+} synthesis in the NAD^{+} stock is required for neutrophil function induced by *Sirt2*$^{-/-}$ following virus infection.

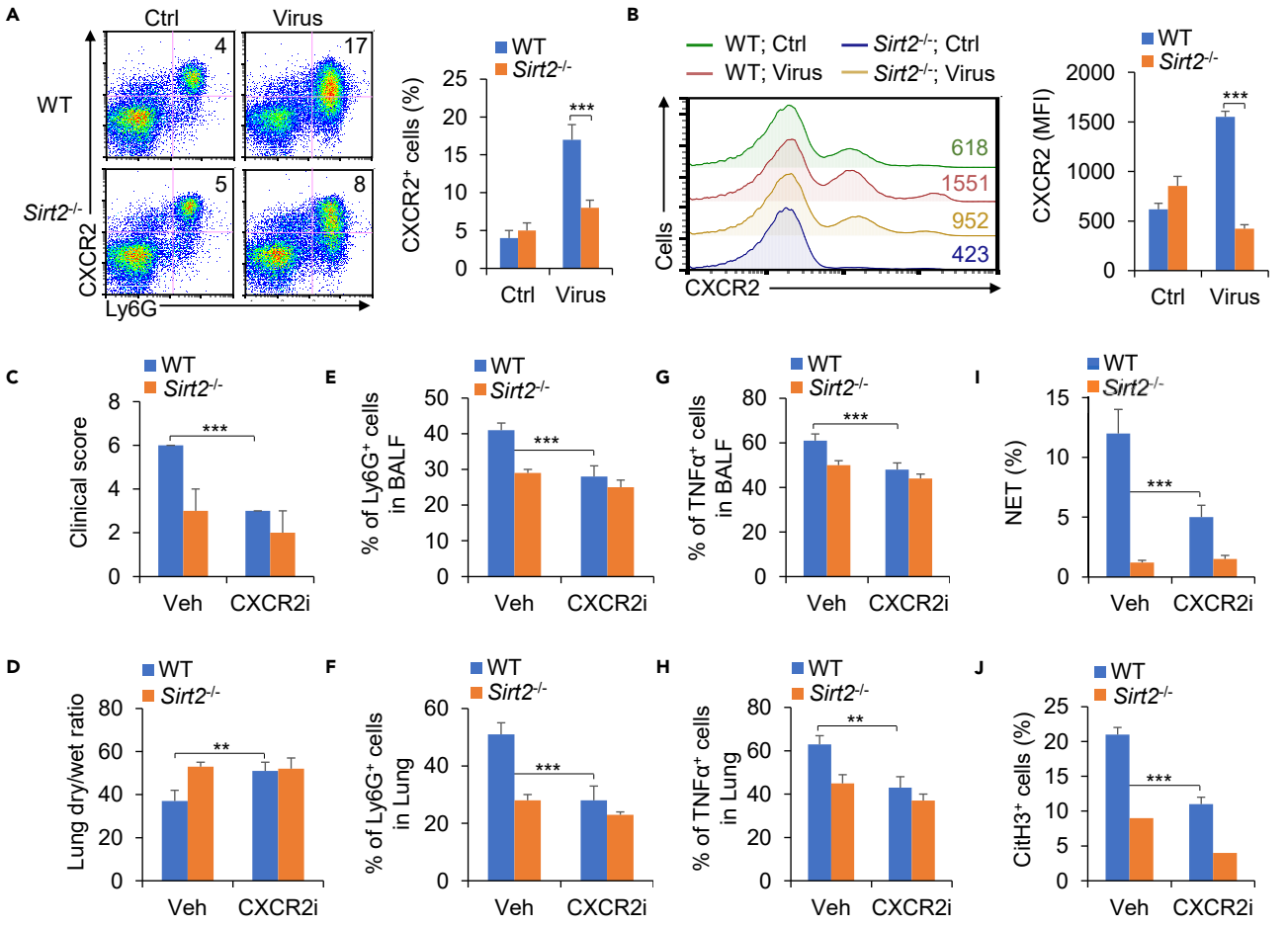

Figure 3. CXCR2 is critically involved in regulating neutrophil function induced by *Sirt2*$^{-/-}$ during virus infection

Percent (A) and mean fluorescent intensity (MFI; B) of CXCR2 surface expressions among CD11b^{+}Ly6G^{+} neutrophils were isolated from bronchoalveolar lavage fluid (BALF) of WT and *Sirt2*$^{-/-}$ mice at 48 h after challenge with PBS (ctrl) or PR8 infection. Representative flow cytometry data (left) and statistical results are shown (right).

(C–J) WT and *Sirt2*$^{-/-}$ mice were challenged with PBS (ctrl) or PR8 virus infection for 48 h with a CXCR2 inhibitor (CXCR2i; SB265610, 5 mg/kg, intraperitoneal injected daily; Tocris Biosciences) or vehicle (PBS). Clinical score of infected mice (C) and the ratio of dry and wet weights of lungs (D) from mice. Percent of CD11b^{+}Ly6G^{+} cells in the BALF (E) and lungs (F) of mice. Intracellular staining of TNF-α in Ly6G^{+} cells in the BALF (G) and lungs (H) of mice. (I) NETs from CD11b^{+}Ly6G^{+} neutrophils were isolated from the BALF of mice. The percent of NET^{+} cells were quantified. (J) Intracellular staining of CitH3 in Ly6G^{+} cells in BALF from mice. The data are representative of three or four independent experiments (n = 3–4 mice per group). **p < 0.01 and ***p < 0.001, compared with the indicated groups.

3-HAO is a key enzyme that catalyzes the synthesis of QA from 3-hydroxy-*o*-aminobenzoic acid. Isolated splenic neutrophils from WT and *Sirt2*$^{-/-}$ mice were stimulated with virus. Consistently, SIRT2 deficiency significantly enhanced the level of QPRT and NAD^{+} (Figures 5I and 5J). Treatment of neutrophils with 3-HAO enhanced the expression of QPRT and the level of NAD^{+} (Figures 5I and 5J). SIRT2 deficiency inhibited NET formation and TNF-α production in neutrophils, but 3-HAO treatment promoted these alterations (Figures 5K and 5L). Altogether, 3-HAO and QPRT are expressed in neutrophils and responsible for NAD^{+} synthesis and neutrophils function induced by *Sirt2*$^{-/-}$ challenged with virus.

TDO and 3-HA are produced in epithelial cells to help neutrophils use QA for NAD^{+} synthesis induced by *Sirt2*$^{-/-}$ following virus infection

As we know,[6] QA is generated through 3-HAO utilizing 3-HA. To determine whether neutrophils can produce 3-HA, we isolated neutrophils from the BALF of infected mice, as well as from the lung tissue, and detected changes in the metabolite 3-HA. SIRT2 deficiency led to decreased 3-HA in neutrophils and increased 3-HA in lung tissue in mice infected with virus (Figures 6A and 6B). Furthermore, analysis of Epcam1^{+} epithelial cells and Epcam1^{-} nonepithelial cells in lung tissue revealed a significant increase in 3-HA production in epithelial cells but not in nonepithelial cells (Figure 6C). These data suggest that 3-HA produced in epithelial cells probably helps neutrophils use QA for NAD^{+} synthesis induced by *Sirt2*$^{-/-}$ during virus infection.

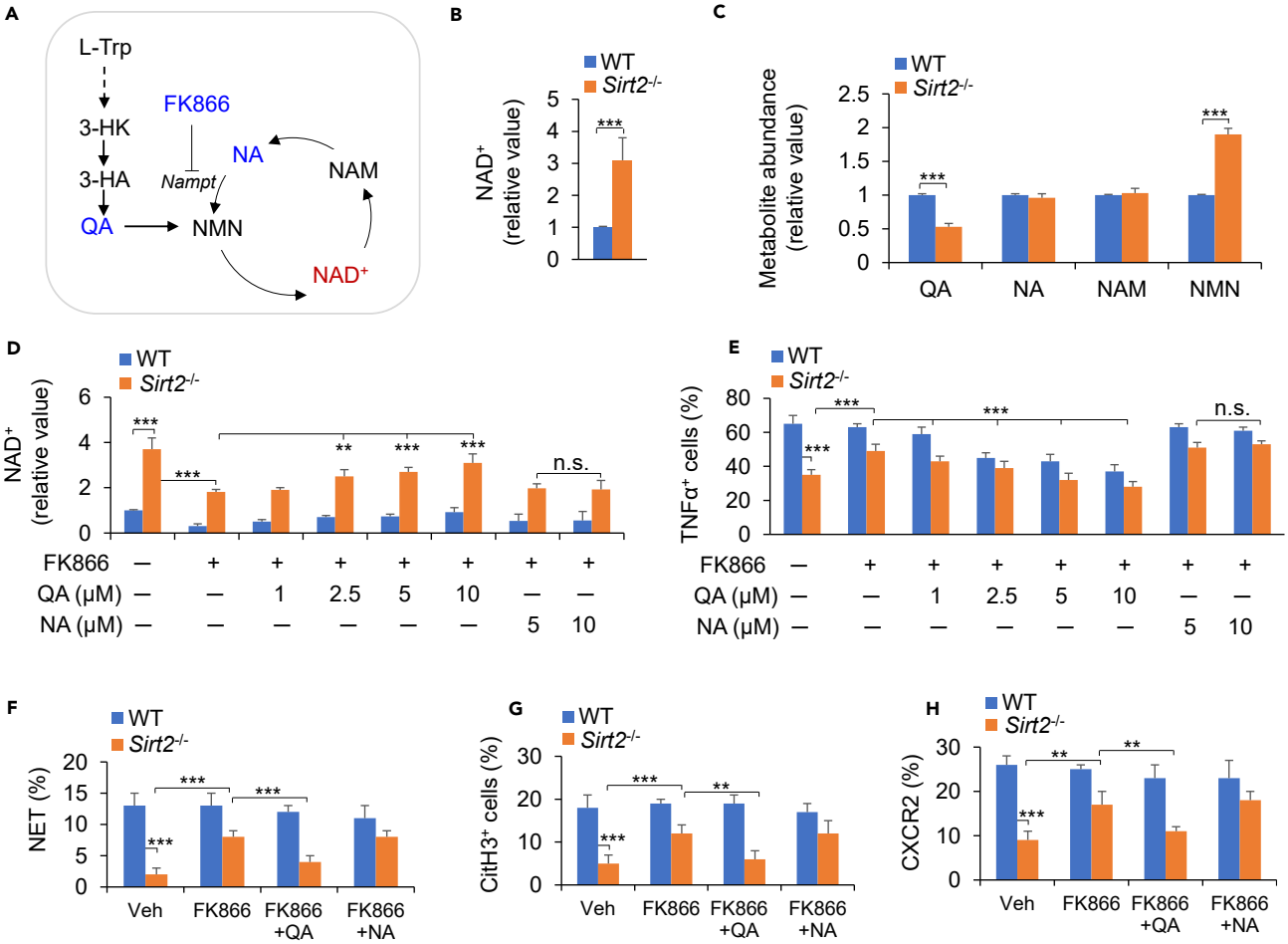

Figure 4. Quinolinic acid constitutes a NAD$^+$ salvage pathway involved in regulating neutrophil function induced by *Sirt2*$^{-/-}$

(A) Quinolinic acid (QA) and the NAD$^+$ salvage pathway.

(B) Changes in the NAD$^+$ level in neutrophils isolated from mouse spleens and stimulated for 24 h with virus.

(C) Mass spectrometry analysis of the metabolite abundance of quinolinic acid (QA), nicotinic acid (NA), NAM, and NMN in CD11b$^+$Ly6G$^+$ neutrophils in the spleens of WT and *Sirt2*$^{-/-}$ mice stimulated for 24 h with the virus.

(D) Changes in the NAD$^+$ level in neutrophils isolated from mouse spleens and stimulated for 24 h with the virus in the presence of FK866 (5 nM, Selleck), QA (1–10 μM, Selleck), or NA (5–10 μM, Selleck).

(E) Intracellular TNFα$^+$ cells among Ly6G$^+$ cells in the spleen of WT and *Sirt2*$^{-/-}$ mice were stimulated for 24 h with virus in the presence of FK866 (5 nM, Selleck), QA (1–10 μM, Selleck), or NA (5–10 μM, Selleck).

(F–H) CD11b$^+$Ly6G$^+$ neutrophils were isolated from the spleens of WT and *Sirt2*$^{-/-}$ mice and stimulated for 24 h with virus in the presence of FK866 (5 nM, Selleck), QA (1–10 μM, Selleck), or NA (5–10 μM, Selleck). (F) The percent of NET$^+$ cells. (G) Intracellular staining of CitH3 in Ly6G$^+$ neutrophils by flow cytometry. (H) Percent of CXCR2 surface expression among Ly6G$^+$ neutrophils determined by flow cytometry. The data are representative of three or four independent experiments (n = 4 mice per group). **$p < 0.01$ and ***$p < 0.001$, compared with the indicated groups. n.s., not significant.

TDO and IDO are crucial for generating 3-HA during Trp metabolism[11] and virus infection also shows changes in their expression.[24,25] We further detected the expression of IDO and TDO in neutrophils and epithelial cells in mice infected with viruses. Interestingly, SIRT2 deficiency led to increased TDO in epithelial cells from lung but not in neutrophils in mice infected with virus (Figures 6D and 6E). These data suggest that TDO expressed in epithelial cells probably supplies 3-HA to neutrophils via QA for NAD$^+$ synthesis induced by *Sirt2*$^{-/-}$ during virus infection.

To test this hypothesis, we established a coculture system of neutrophils and epithelial cells treated with or without the TDO inhibitor (Figure 6F). SIRT2 deficiency enhanced the NAD$^+$ level and led to sustained alterations, but epithelial supernatant supplementation advanced the peak NAD$^+$ level and lasted for a longer time. However, epithelial cells treated with the TDO inhibitor recovered these effects to control levels (Figure 6G). Neutrophil TNFα production also exhibited similar alterations (Figure 6H). Importantly, *Sirt2*$^{-/-}$ neutrophils treated by epithelial supernatant enhanced the level of 3-HA (Figures S6A and S6B) and lowered neutrophils NET formation and proinflammatory cytokine TNFα production and showed consistent tendency with 3-HA treatment (Figures S6B and S6E), which indicating 3-HA may be one of components in the epithelial supernatant, playing a key regulatory role on neutrophil functions induced by *Sirt2*$^{-/-}$ during virus infection. Taken together,

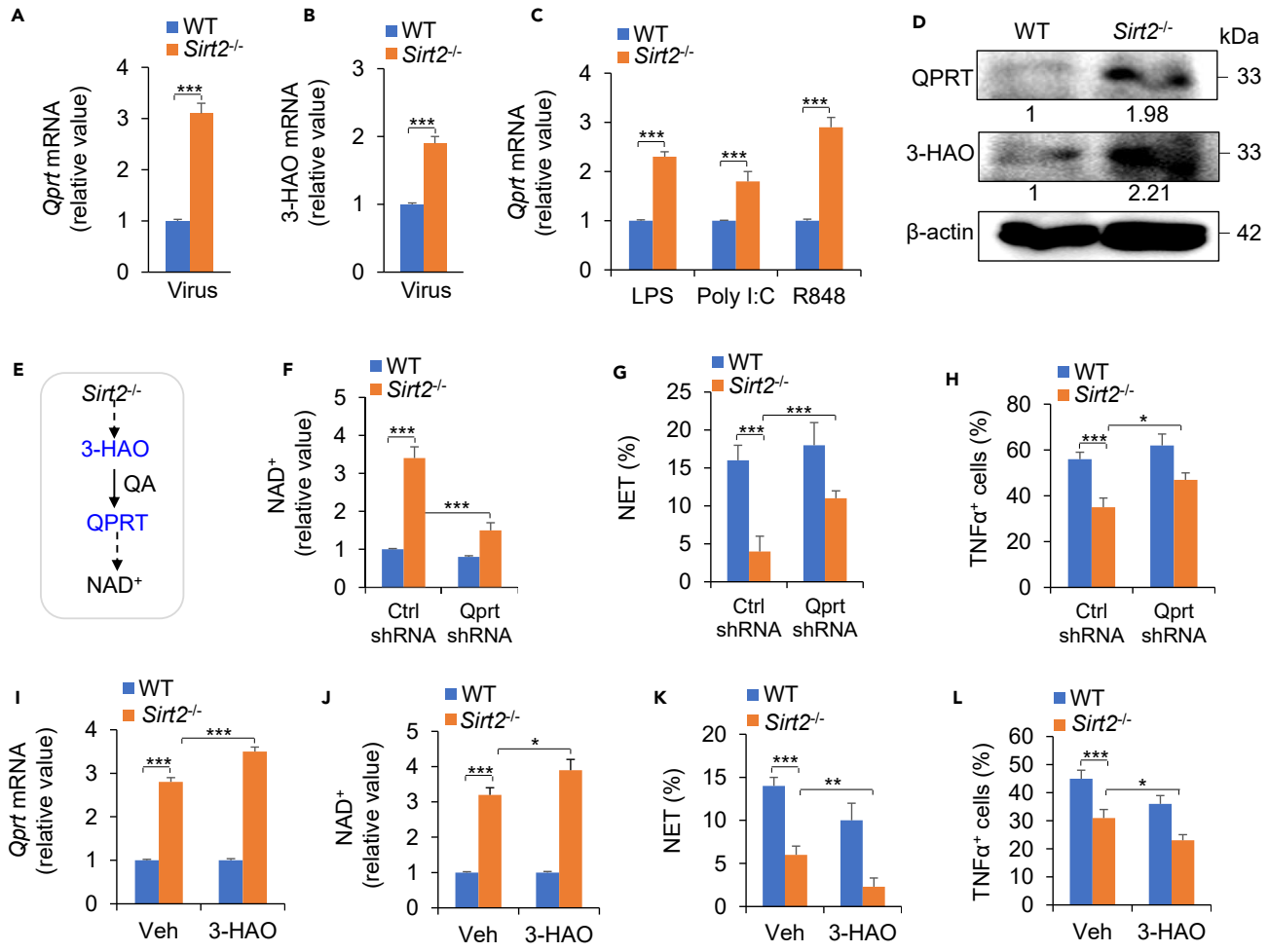

Figure 5. QPRT is expressed in neutrophils and is responsible for NAD$^+$ synthesis induced by *Sirt2*$^{-/-}$

(A and B) WT and *Sirt2*$^{-/-}$ mice were challenged with the PR8 virus at 48 h. *Qprt* mRNA (A) and *3-HAO* mRNA expression in neutrophils isolated from BALF in mice.

(C) *Qprt* mRNA expression in neutrophils isolated from mouse spleens and stimulated for 24 h with 1 μg/mL LPS, 30 μg/mL Poly I:C and 5 μg/mL R848 (all from Sigma).

(D) Western blot of QPRT and 3-HAO in neutrophils from BALF from WT and *Sirt2*$^{-/-}$ mice challenged with the PR8 virus at 48 h.

(E) QPRT and 3-HAO for the NAD$^+$ synthesis pathway.

(F–H) Neutrophils isolated from the spleens of WT and *Sirt2*$^{-/-}$ mice and transfected with lentivirus containing control vector small interfering RNA (siRNA ctrl) or the Qprt gene (siRNA Qprt) were stimulated for 24 h by the virus. Changes in the NAD$^+$ level (F), percent of NET$^+$ cells (G) and intracellular staining for TNF-α (H) in Ly6G$^+$ neutrophils transfected with siCtrl and siQprt.

(I–L) CD11b$^+$Ly6G$^+$ neutrophils were isolated from the spleens of WT and *Sirt2*$^{-/-}$ mice and stimulated for 24 h with virus in the presence of 3-hydroxyanthranilate 3,4-dioxygenase (3-HAO, 2 nM, MCE). *Qprt* mRNA expression (I), changes in NAD$^+$ levels (J), percent of NET$^+$ cells (K) and intracellular staining of TNFα in Ly6G$^+$ neutrophils determined via flow cytometry (L). The data are representative of three or four independent experiments ($n = 4$ mice per group). *$p < 0.05$, **$p < 0.01$ and ***$p < 0.001$, compared with the indicated groups.

these data reveal that TDO and 3-HA produced by epithelial cells help neutrophils use QA to reduce the NAD$^+$ stock induced by *Sirt2*$^{-/-}$ during virus infection.

Pharmacologically targeting SIRT2 and QA in the regulation of mouse and human neutrophil functions

Next, we tested the use of a pharmacological approach to target SIRT2 and QA in mice and determined whether our findings could be recapitulated through the use of the genetic target SIRT2 and the NAD$^+$ synthesis pathway (Figure 7A). Blocking SIRT2 with its inhibitor AGK2 significantly ameliorated lung tissue inflammatory injury and inhibited neutrophil infiltration into the lung and the production of the proinflammatory cytokine TNF-α in neutrophils from mice infected with the virus (Figures 7B–7E). However, in combination with treatment with the

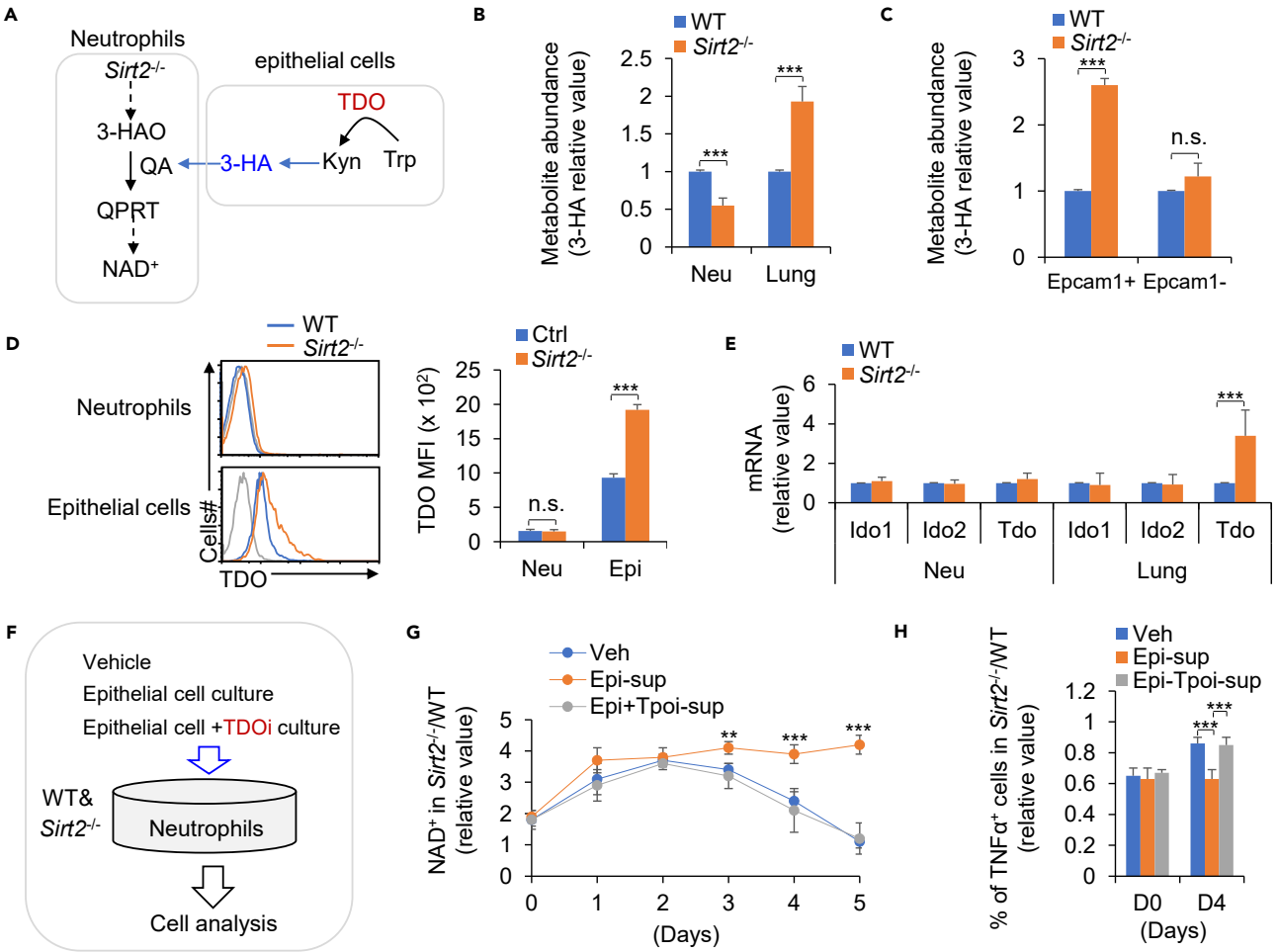

Figure 6. Epithelial cells help neutrophils use QA for NAD^+ synthesis induced by *Sirt2*$^{-/-}$ following virus infection

(A) TDO and 3-HA in the NAD^+ synthesis pathway.

(B) Single-cell suspension was prepared from lung tissue. Mass spectrometry analysis of the metabolite abundance of 3-HA in neutrophils from BALF and in lung tissue from WT and *Sirt2*$^{-/-}$ mice challenged with the PR8 virus at 48 h.

(C) Mass spectrometry analysis of the metabolite abundance of 3-HA in Epcam1$^+$ and Epicam1$^-$ cells from lung tissue from WT and *Sirt2*$^{-/-}$ mice challenged by PR8 virus infection at 48 h.

(D) Flow cytometry analysis of TDO expression in neutrophils and epithelial cells in the lungs of WT and *Sirt2*$^{-/-}$ mice challenged with the PR8 virus at 48 h.

(E) *Ido1/2* and *Tdo* mRNA expression of neutrophils or cells from lung tissue from WT and *Sirt2*$^{-/-}$ mice challenged by PR8 virus infection at 48 h.

(F–H) Neutrophils were isolated from the spleens of WT and *Sirt2*$^{-/-}$ mice cocultured with vehicle (in PBS), epithelial cells or epithelial cells treated with a TDO inhibitor (LM10, 10 nM, MCE) and stimulated with virus for different durations. Ratio of the NAD^+ level in *Sirt2*$^{-/-}$ and WT mice (G) and the ratio of TNF-α^+ cells in neutrophils from *Sirt2*$^{-/-}$ and WT mice (H). The data are representative of three or four independent experiments (n = 3–4 mice per group). $^{**}p < 0.01$ and $^{***}p < 0.001$, compared with the indicated groups. n.s., not significant.

NAMPT inhibitor FK866, the NAD^+ level was lower and neutrophil infiltration and TNF-α production were enhanced. Furthermore, combination treatment with QA restored NAD^+ levels and inhibited neutrophil infiltration and TNF-α production (Figures 7B–7E, S7A, and S7B).

We further tested the role of SIRT2 in human neutrophils, which are generated from human CD34$^+$ hematopoietic stem cells induced by G-CSF for 7 days (Figure 7F). Blocking SIRT2 with AGK2 reduced SIRT2 expression and the production of TNF-α in neutrophils (Figures 7G and 7H). Additionally, AGK2 treatment enhanced the expression of *Qprt* and *Nampt* (Figure 7I). Thus, our data demonstrated that the SIRT2-quinolinic acid-QPRT-mediated NAD^+ synthesis pathway is an evolutionarily conserved signaling pathway that regulates mouse and human neutrophil functional activities.

DISCUSSION

The Trp-to-QA pathway has been shown to be critical in several psychiatric conditions, such as depression and stress-related disorders.[1–3,26] QA can direct a portion of Trp catabolism toward replenishing NAD^+ levels in response to inflammation.[27] However, the roles of the

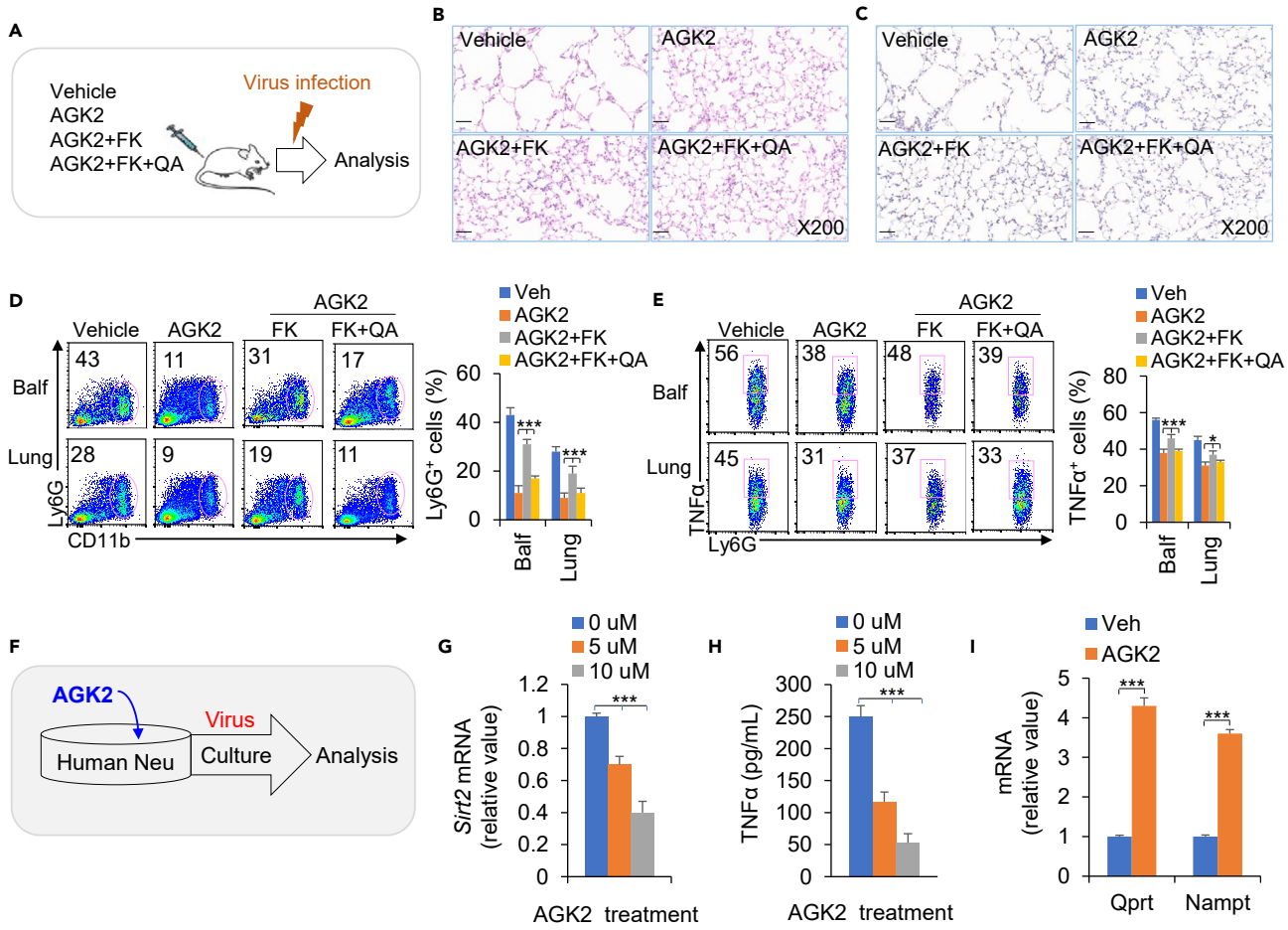

Figure 7. SIRT2 deficiency inhibits neutrophil functions through the QA-QPRT-NAD$^+$ synthesis pathway

(A–F) WT mice were challenged with the PR8 virus at 48 h and treated with PBS (vehicle), AGK2 (5 mg/kg, Selleck), AGK2+FK866 (10 mg/kg, Selleck) or AGK2+FK866+QA (10 mg/kg, Selleck) (A). (B) Hematoxylin and eosin (H&E) staining of mouse lungs at 48 h after challenge with the PR8 virus. (C) Immunohistochemical staining of anti-Ly6G in the lungs at 48 h after challenge with the PR8 virus. (D) Flow cytometry analysis of CD11b$^+$Ly6G$^+$ cells in the BALF or lungs of WT mice challenged with the PR8 virus at 48 h. Dot plots present representative flow cytometry data (left), and the statistical results are shown (right). (E) Intracellular staining of TNF-α in CD11b$^+$Ly6G$^+$ cells in the BALF or lungs of WT mice challenged with the PR8 virus at 48 h. Dot plots present representative flow cytometry data (left), and the statistical results are shown (right).

(F–I) Human CD34$^+$ hematopoietic stem cells were induced with G-CSF (10 ng/mL, Sigma) for 7 days. Neutrophils were treated with AGK2 (0–10 μM, Selleck) at the indicated dose and stimulated with virus for 24 h (F). (G) *Sirt2* mRNA expression in neutrophils. (H) TNF-α production in the supernatant, as determined by ELISA. (I) *Qprt* and *Nampt* mRNA expression in neutrophils. The data are representative of three or four independent experiments ($n = 3$ per group). *$p < 0.05$ and ***$p < 0.001$, compared with the indicated groups.

tryptophan metabolite QA and the QA-NAD$^+$ pathway in preventing viral infection in neutrophils have not been determined. SIRT2 is an NAD$^+$-dependent class III histone deacetylase and is emerging as a crucial regulator of T cell-mediated adaptive immunity.[15] Although it has been proposed that SIRT2 has a central role in some diseases, its specific function remains controversial. Herein, our data showed that QPRT mediated the switch in NAD$^+$ metabolism by exploiting neutrophil-derived QA as an alternative source of replenished intracellular NAD$^+$ pools induced by *Sirt2*$^{-/-}$ to regulate neutrophil functions during virus infection, with implications for future immunotherapy approaches (Figure S8).

The constitutive catabolism of Trp in various types of cancer helps to suppress antitumor immunity.[5,11] Therefore, the Trp pathway, which is driven by the inhibition of IDO-1, has been identified as a therapeutic target for cancer-related immunosuppression and cancer and autoimmune-mediated inflammation.[28] The IDO-1 inhibitor has entered clinical trials.[29,30] Tryptophan 2,3-dioxygenase (TDO) is expressed in the liver and in glioma, but limited research has been conducted on this topic. QA accumulates in neurodegenerative and inflammatory central nervous system (CNS) diseases and is an endogenous ligand of N-methyl-D-aspartate (NMDA) receptors that induces neuronal damage through excitotoxicity.[9] However, the role of the Trp-quinolinic acid-QPRT signaling pathway in neutrophils challenged by viral infection has not been reported. Importantly, TDO, but not IDO, is expressed in epithelial cells but not in neutrophils and is crucial for generating 3-HA during Trp metabolism. Neutrophils treated by epithelial supernatant enhanced the level of 3-HA and lowered neutrophils functions

and showed consistent tendency with 3-HA treatment. These indicate that 3-HA is probably the one of the components in the epithelial supernatant and plays critical regulatory role on neutrophil function during viral infection. However, the mechanism by which 3-HA enters neutrophils through diffusion, receptor mediation or other pathways is still unclear and requires further research. Thus, this finding provides insight into the collaborative regulatory mechanism of SIRT2 in neutrophils and epithelial cells during viral infection. A new mechanism for regulating the immune response of neutrophils to viral infections can be achieved by utilizing the epithelial cell 3-HA to regulate the internal NAD^+ stock of neutrophils.

The targeting effect of FK866 (a NAMPT inhibitor) on the novel NAD^+ synthesis pathway increases the sensitivity of tumor cells to apoptosis, and FK866 is currently being evaluated in phase II clinical trials for cancer patients.[31] Although the results of therapeutic NAD^+ depletion are promising, the inhibitory effect of NAMPT may be influenced by the activity of QA- and NA-dependent NAD^+ synthesis pathways. Both QA and NA can serve as alternative substrates for NAD^+ synthesis. Our data showed that SIRT2 deficiency enhanced 3-HAO and QPRT expression and exploited QA as an alternative source of replenished intracellular NAD^+ pools induced by *Sirt2*$^{-/-}$ to regulate neutrophil functions during virus infection, with implications for future immunotherapy approaches.

SIRT2 is a cytosolic NAD^+-dependent class III histone deacetylase that is emerging as a crucial regulator of T cell-mediated adaptive immunity.[32] It is known to shuttle to the nucleus during mitosis and certain bacterial infections. They play a considerable role in critical cellular processes such as cellular metabolism, cellular homeostasis, tumor suppression, and inflammation.[15–18] Although it has been proposed that SIRT2 has a central role in some diseases. However, whether SIRT2 has a regulatory effect on the antiviral infection ability of neutrophils and its underlying mechanism are unclear. Our data showed that SIRT2 deficiency in neutrophils inhibited the infiltration of neutrophils in BALF and lung tissue, as well as the secretion of inflammatory cytokines and the formation of NETs, ameliorating disease symptoms during acute respiratory virus infection. Additionally, CXCR2 is required for NET formation and neutrophil functional activity induced by *Sirt2*$^{-/-}$ during virus infection. This finding provides a clear regulatory pathway for targeting SIRT2 signaling to regulate neutrophil function during antiviral infection.

In summary, the NAD^+-dependent histone deacetylase SIRT2 is a key regulator of neutrophil functional activities. Additionally, QA-QPRT pathways, which are alternative sources of NAD^+ that replenish intracellular NAD^+ pools, are important for regulating the functions of neutrophils induced by *Sirt2*$^{-/-}$ during antiviral infection.

Limitations of the study

Although we have demonstrated that SIRT2 can regulate neutrophil function and play a key regulatory role in antiviral immunity. However, the triggering mechanism of SIRT2 is still unclear. Further research is needed on the upstream signaling of SIRT2. When the virus invades, how does the virus induce changes in SIRT2 expression and alter neutrophil immune responses. These will help to study antiviral immune intervention therapies targeting neutrophil SIRT2.

STAR★METHODS

Detailed methods are provided in the online version of this paper and include the following:

- KEY RESOURCES TABLE
- RESOURCE AVAILABILITY
  - Lead contact
  - Materials availability
  - Data and code availability
- EXPERIMENTAL MODEL AND STUDY PARTICIPANT DETAILS
  - Animal studies
  - Viral infection model
  - Consent for publication
- METHOD DETAILS
  - Histopathological analyses
  - Neutrophil isolation and culture
  - NET formation assay
  - Flow cytometry
  - Targeted metabolomics analysis
  - Immunoblot assays
  - Quantitative RT-PCR
  - RNA sequences
  - QPRT silenced by RNA interference
  - NAD^+ level assay
  - ELISA
  - Human cell culture
- QUANTIFICATION AND STATISTICAL ANALYSIS

SUPPLEMENTAL INFORMATION

Supplemental information can be found online at https://doi.org/10.1016/j.isci.2024.110184.

ACKNOWLEDGMENTS

The authors' research is supported by grants from the National Natural Science Foundation for Key Programs of China (31730024, G.L.), National Natural Science Foundation for General Programs of China (32170911 and 32370924, G.L.) and Beijing Municipal Natural Science Foundation of China (5202013, G.L.).

AUTHOR CONTRIBUTIONS

Z.Z., Y.Q., D.Y., and W.L. designed and conducted the experiment with cells and mice, analyzed data; N.R. and X.J. participated in the discussions, B.Y. contributed to writing the manuscript and participated in discussions, L.G. developed the concept, designed and conducted the experiments, analyzed data, wrote the manuscript, and provided overall direction.

DECLARATION OF INTERESTS

The authors declare no competing interests.

Received: January 11, 2024
Revised: April 12, 2024
Accepted: June 1, 2024
Published: June 4, 2024

REFERENCES

1. Gargaro, M., Scalisi, G., Manni, G., Briseño, C.G., Bagadia, P., Durai, V., Theisen, D.J., Kim, S., Castelli, M., Xu, C.A., et al. (2022). Indoleamine 2,3-dioxygenase 1 activation in mature cDC1 promotes tolerogenic education of inflammatory cDC2 via metabolic communication. Immunity *55*, 12.
2. Sheibani, M., Shayan, M., Khalilzadeh, M., Soltani, Z.E., Jafari-Sabet, M., Ghasemi, M., and Dehpo, A.R. (2023). Kynurenine pathway and its role in neurologic, psychiatric, and inflammatory bowel diseases. Mol. Biol. Rep. *50*, 16.
3. Xiu, X., Puskar, N.L., Shanata, J.A.P., Lester, H.A., and Dougherty, D.A. (2009). Nicotine binding to brain receptors requires a strong cation-pi interaction. Nature *458*, 3.
4. Ahmed, S., Somarribas Patterson, L.F., Öztürk, S., Mohapatra, S.R., Panitz, V., Secker, P.F., Pfänder, P., Loth, S., Salem, H., Prentzell, M.T., et al. (2020). IL4I1 Is a Metabolic Immune Checkpoint that Activates the AHR and Promotes Tumor Progression. Cell *182*, 18.
5. Preston, W.A., Pace, D.J., Altshuler, P.J., Yi, M., Kittle, H.D., Vincent, S.A., Andreoni, K.A., Frank, A.M., Glorioso, J.M., Ramirez, C.G., et al. (2024). A propensity score matched analysis of liver transplantation outcomes in the setting of preservation solution shortage. Am. J. Transplant. *24*, 619–630.
6. Dang, H., Castro-Portuguez, R., Espejo, L., Backer, G., Freitas, S., Spence, E., Meyers, J., Shuck, K., Gardea, E.A., Chang, L.M., et al. (2023). On the benefits of the tryptophan metabolite 3-hydroxyanthranilic acid in Caenorhabditis elegans and mouse aging. Nat. Commun. *14*, 8338.
7. Kesarwani, P., Kant, S., Zhao, Y., Prabhu, A., Buelow, K.L., Miller, C.R., and Chinnaiyan, P. (2023). Quinolinate promotes macrophage-induced immune tolerance in glioblastoma through the NMDAR/PPARγ signaling axis. Nat. Commun. *14*, 1459.
8. Huang, J., Liu, D., Wang, Y., Liu, L., Li, J., Yuan, J., Jiang, Z., Jiang, Z., Hsiao, W.W., Liu, H., et al. (2022). Ginseng polysaccharides alter the gut microbiota and kynurenine/tryptophan ratio, potentiating the antitumour effect of antiprogrammed cell death 1/programmed cell death ligand 1 (anti-PD-1/PD-L1) immunotherapy. Gut *71*, 734–745.
9. Bakker, L., Ramakers, I.H.G.B., J P M Eussen, S., Choe, K., van den Hove, D.L.A., Kenis, G., Rutten, B.P.F., van Oostenbrugge, R.J., Staals, J., Ulvik, A., et al. (2023). The role of the kynurenine pathway in cognitive functioning after stroke: A prospective clinical study. J. Neurol. Sci. *454*, 120819.
10. Kesarwani, P., Prabhu, A., Kant, S., and Chinnaiyan, P. (2019). Metabolic remodeling contributes towards an immune-suppressive phenotype in glioblastoma. Cancer Immunol. Immunother. *68*, 13.
11. Kesarwani, P., Prabhu, A., Kant, S., Kumar, P., Graham, S.F., Buelow, K.L., Wilson, G.D., Miller, C.R., and Chinnaiyan, P. (2018). Tryptophan Metabolism Contributes to Radiation-Induced Immune Checkpoint Reactivation in Glioblastoma. Clin. Cancer Res. *24*, 11.
12. Kesarwani, P., Kant, S., Zhao, Y., Prabhu, A., Buelow, K.L., Miller, C.R., and Chinnaiyan, P. (2023). Quinolinate promotes macrophage-induced immune tolerance in glioblastoma through the NMDAR/PPARγ signaling axis. Nat. Commun. *14*, 1459.
13. Hestad, K., Alexander, J., Rootwelt, H., and Aaseth, J.O. (2022). The Role of Tryptophan Dysmetabolism and Quinolinic Acid in Depressive and Neurodegenerative Diseases. Biomolecules *12*, 998.
14. Sugisawa, E., Kondo, T., Kumaga, Y., Kato, H., Takayama, Y., Isohashi, K., Shimosegawa, E., Takemura, N., Hayashi, Y., Sasaki, T., et al. (2022). Nociceptor-derived Reg3γ prevents endotoxic death by targeting kynurenine pathway in microglia. Cell Rep. *38*, 110462.
15. Hamaidi, I., Zhang, L., Kim, N., Wang, M.H., Iclozan, C., Fang, B., Liu, M., Koomen, J.M., Berglund, A.E., Yoder, S.J., et al. (2020). Sirt2 Inhibition Enhances Metabolic Fitness and Effector Functions of Tumor-Reactive T Cells. Cell Metab. *32*, 420–436.e12. https://doi.org/10.1016/j.cmet.2020.07.008.
16. Bai, N., Li, N., Cheng, R., Guan, Y., Zhao, X., Song, Z., Xu, H., Yi, F., Jiang, B., Li, X., et al. (2022). Inhibition of SIRT2 promotes APP acetylation and ameliorates cognitive impairment in APP/PS1 transgenic mice. Cell Rep. *40*, 111062. https://doi.org/10.1016/j.celrep.2022.111062.
17. Wang, B., Ye, Y., Yang, X., Liu, B., Wang, Z., Chen, S., Jiang, K., Zhang, W., Jiang, H., Mustonen, H., et al. (2020). SIRT2-dependent IDH1 deacetylation inhibits colorectal cancer and liver metastases. EMBO Rep. *21*, e48183. https://doi.org/10.15252/embr.201948183.
18. Shin, J., Zhang, D., and Chen, D. (2011). Reversible acetylation of metabolic enzymes celebration: SIRT2 and p300 join the party. Mol. Cell *43*, 3–5. https://doi.org/10.1016/j.molcel.2011.06.010.
19. Sarikhani, M., Mishra, S., Desingu, P.A., Kotyada, C., Wolfgeher, D., Gupta, M.P., Singh, M., and Sundaresan, N.R. (2018). SIRT2 regulates oxidative stress-induced cell death through deacetylation of c-Jun NH(2)-terminal kinase. Cell Death Differ. *25*, 1638–1656. https://doi.org/10.1038/s41418-018-0069-8.
20. Honda, M., and Kubes, P. (2018). Neutrophils and neutrophil extracellular traps in the liver and gastrointestinal system. Nat. Rev. Gastroenterol. Hepatol. *15*, 206–221. https://doi.org/10.1038/nrgastro.2017.183.
21. Boldenow, E., Gendrin, C., Ngo, L., Bierle, C., Vornhagen, J., Coleman, M., Merillat, S., Armistead, B., Whidbey, C., Alishetti, V., et al. (2016). Group B Streptococcus circumvents neutrophils and neutrophil extracellular traps during amniotic cavity invasion and preterm

labor. Sci. Immunol. *1*, eaah4576. https://doi.org/10.1126/sciimmunol.aah4576.

22. Chan, L., Karimi, N., Morovati, S., Alizadeh, K., Kakish, J.E., Vanderkamp, S., Fazel, F., Napoleoni, C., Alizadeh, K., Mehrani, Y., et al. (2021). The Roles of Neutrophils in Cytokine Storms. Viruses *13*, 2318. https://doi.org/10.3390/v13112318.
23. Metzler, K.D., Goosmann, C., Lubojemska, A., Zychlinsky, A., and Papayannopoulos, V. (2014). A myeloperoxidase-containing complex regulates neutrophil elastase release and actin dynamics during NETosis. Cell Rep. *8*, 883–896. https://doi.org/10.1016/j.celrep.2014.06.044.
24. Badawy, A.A.-B. (2023). The kynurenine pathway of tryptophan metabolism: a neglected therapeutic target of COVID-19 pathophysiology and immunotherapy. Biosci. Rep. *43*, BSR20230595.
25. Venancio, P.A., Consolaro, M.E.L., Derchain, S.F., Boccardo, E., Villa, L.L., Maria-Engler, S.S., Campa, A., and Discacciati, M.G. (2019). Indoleamine 2,3-dioxygenase and tryptophan 2,3-dioxygenase expression in HPV infection, SILs, and cervical cancer. Cancer Cytopathol. *127*, 11.
26. Yu, K., Li, Q., Sun, X., Peng, X., Tang, Q., Chu, H., Zhou, L., Wang, B., Zhou, Z., Deng, X., et al. (2023). Bacterial indole-3-lactic acid affects epithelium-macrophage crosstalk to regulate intestinal homeostasis. Proc. Natl. Acad. Sci. USA *120*, 11.
27. Shi, X., Zhao, G., Li, H., Zhao, Z., Li, W., Wu, M., and Du, Y.L. (2023). Hydroxytryptophan biosynthesis by a family of heme-dependent enzymes in bacteria. Nat. Chem. Biol. *19*, 1415–1422.
28. Labadie, B.W., Bao, R., and Luke, J.J. (2019). Reimagining IDO Pathway Inhibition in Cancer Immunotherapy via Downstream Focus on the Tryptophan-Kynurenine-Aryl Hydrocarbon Axis. Clin. Cancer Res. *25*, 11.
29. Zhai, L., Ladomersky, E., Lenzen, A., Nguyen, B., Patel, R., Lauing, K.L., Wu, M., and Wainwright, D.A. (2018). IDO1 in cancer: a Gemini of immune checkpoints. Cell. Mol. Immunol. *15*, 10.
30. Fujiwara, Y., Kato, S., Nesline, M.K., Conroy, J.M., DePietro, P., Pabla, S., and Kurzrock, R. (2022). Indoleamine 2,3-dioxygenase (IDO) inhibitors and cancer immunotherapy. Cancer Treat Rev. *110*, 21.
31. Gerner, R.R., Macheiner, S., Reider, S., Siegmund, K., Grabherr, F., Mayr, L., Texler, B., Moser, P., Effenberger, M., Schwaighofer, H., et al. (2020). Targeting NAD immunometabolism limits severe graft-versus-host disease and has potent antileukemic activity. Leukemia *34*, 12.
32. Wu, M., Zhang, J.B., Xiong, Y.W., Zhao, Y.X., Zheng, M.G., Huang, X.L., Huang, F., Wu, X.X., Li, X., Fan, W.J., et al. (2023). Promotion of Lung Cancer Metastasis by SIRT2-Mediated Extracellular Protein Deacetylation. Adv. Sci. *10*, e2205462. https://doi.org/10.1002/advs.202205462.
33. Dong, L., Cao, Y., Yang, H., Hou, Y., He, Y., Wang, Y., Yang, Q., Bi, Y., and Liu, G. (2023). The hippo kinase MST1 negatively regulates the differentiation of follicular helper T cells. Immunology *168*, 511–525. https://doi.org/10.1111/imm.13590.
34. Kadl, A., Pontiller, J., Exner, M., and Leitinger, N. (2007). Single bolus injection of bilirubin improves the clinical outcome in a mouse model of endotoxemia. Shock *28*, 582–588. https://doi.org/10.1097/shk.0b013e31804d41dd.
35. Zhang, N., Zhang, Y., You, S., Tian, Y., Lu, S., Cao, L., and Sun, Y. (2020). Septin4 Prevents PDGF-BB-induced HAVSMC Phenotypic Transformation, Proliferation and Migration by Promoting SIRT1-STAT3 Deacetylation and Dephosphorylation. Int. J. Biol. Sci. *16*, 708–718. https://doi.org/10.7150/ijbs.39843.
36. Liu, G., Hu, X., Sun, B., Yang, T., Shi, J., Zhang, L., and Zhao, Y. (2013). Phosphatase Wip1 negatively regulates neutrophil development through p38 MAPK-STAT1. Blood *121*, 519–529. https://doi.org/10.1182/blood-2012-05-432674.
37. Liu, G., Bi, Y., Wang, R., Shen, B., Zhang, Y., Yang, H., Wang, X., Liu, H., Lu, Y., and Han, F. (2013). Kinase AKT1 negatively controls neutrophil recruitment and function in mice. J. Immunol. *191*, 2680–2690. https://doi.org/10.4049/jimmunol.1300736.
38. Cichon, I., Santocki, M., Ortmann, W., and Kolaczkowska, E. (2020). Imaging of Neutrophils and Neutrophil Extracellular Traps (NETs) with Intravital (In Vivo) Microscopy. Methods Mol. Biol. *2087*, 443–466. https://doi.org/10.1007/978-1-0716-0154-9_26.
39. Li, C., Bi, Y., Li, Y., Yang, H., Yu, Q., Wang, J., Wang, Y., Su, H., Jia, A., Hu, Y., et al. (2017). Dendritic cell MST1 inhibits Th17 differentiation. Nat. Commun. *8*, 14275. https://doi.org/10.1038/ncomms14275.
40. Yan, Y., Chang, L., Tian, H., Wang, L., Zhang, Y., Yang, T., Li, G., Hu, W., Shah, K., Chen, G., and Guo, Y. (2018). 1-Pyrroline-5-carboxylate released by prostate Cancer cell inhibit T cell proliferation and function by targeting SHP1/cytochrome c oxidoreductase/ROS Axis. J. Immunother. Cancer *6*, 148.
41. Wang, Y., Yang, H., Jia, A., Wang, Y., Yang, Q., Dong, Y., Hou, Y., Cao, Y., Dong, L., Bi, Y., and Liu, G. (2022). Dendritic cell Piezo1 directs the differentiation of TH1 and Treg cells in cancer. Elife *11*, e79957. https://doi.org/10.7554/eLife.79957.
42. Li, Y., Jia, A., Yang, H., Wang, Y., Wang, Y., Yang, Q., Cao, Y., Bi, Y., and Liu, G. (2022). Protein Tyrosine Phosphatase PTPRO Signaling Couples Metabolic States to Control the Development of Granulocyte Progenitor Cells. J. Immunol. *208*, 1434–1444. https://doi.org/10.4049/jimmunol.2100878.

STAR★METHODS

KEY RESOURCES TABLE

REAGENT or RESOURCE	SOURCE	IDENTIFIER
Antibodies		
Anti-Ly6G PE	Abcam	Cat# ab25378, RRID: AB_470493
Anti-CD11b-FITC	Biolegend	Cat# 301330 (also 301329); RRID: AB_2561703
Alexa Fluor® 488-conjugated anti-rabbit IgG (H + L)	Abcam	Cat# ab150077; RRID: AB_2922865
Anti-TCR FITC	Abcam	Cat# ab25010; RRID: AB_2619709
Anti-CD45 APC	Abcam	Cat# ab210182; RRID: AB_929195
Anti-CD44 PE	Abcam	Cat# ab23396; RRID: AB_10763149
Anti-CD62L FITC	Abcam	Cat# 24876; RRID: AB_10760977
Anti-CD4 APC-Cy7	Abcam	Cat# 233298; RRID: AB_10015166
Anti-CD8α APC	Abcam	Cat# 237368; RRID: AB_10781971
Anti-histone H3 (citrulline R2+R8+R17)	Abcam	Cat# ab5103; RRID: AB_11214865
Anti-SIRT2	Abcam	Cat# ab51023; RRID: AB_1193120
Anti-NAMPT	Abcam	Cat# ab236874; RRID: AB_2490117
Anti-QPRT	ThermoFisher Scientific	Cat# PA5-110251; RRID: AB_10836833
Anti-3-HAO	ThermoFisher Scientific	Cat# PA5-20774
Anti-TDO	Abcam	Cat# 259359; RRID: AB_2475964
Anti-β-actin	Abcam	Cat# ab6276; RRID: AB_10834148
Anti-GAPDH	Abcam	Cat# 8245; RRID: AB_2722713
Anti-CXCR2	R&D systems	Cat# FAB2164P; RRID: AB_10386449
Anti-IL-10 APC	Biolegend	Cat# JES5-16E3; RRID: AB_11181697
Anti-TNFα APC	Biolegend	Cat# MP6-XT22; RRID: AB_2943277
Bacterial and virus strains		
Mouse-adapted influenza virus strain A/Puerto Rico/8/34	Sino Biological, Inc. (China)	N/A
Chemicals, peptides, and recombinant proteins		
ACK Lysis Buffer	ThermoFisher Scientific	Cat# A10492-01
AGK2	Selleck	N/A
BSA (Bovine serum albumin)	Sigma-Aldrich	Cat# 05470
DMEM	ThermoFisher Scientific	Cat# 11965092
EDTA	Invitrogen	Cat# 15575-020
Fetal bovine serum	ThermoFisher Scientific	Cat# 16000044
Fetal calf serum	ThermoFisher Scientific	Cat# 16140071
FK866	Selleck	N/A
G-CSF	PeproTech	Cat# BE0259-1MG
3-HA	MCE	Cat# HY-W001171
3-HAO	MCE	Cat# HY-P76963
HEPES	ThermoFisher Scientific	Cat# 15630-080
Hoechst 33342	Beyotime	Cat#C1011
10X RIPA Buffer	Cell Signaling	Cat# 9806
β-mercaptoethanol	Sigma	Cat# M3148
NAD^+	Selleck	N/A

(*Continued on next page*)

Continued

REAGENT or RESOURCE	SOURCE	IDENTIFIER
Nicotinic acid (NA)	Selleck	N/A
0.45 mm nitrocellulose membrane	Cytiva	Cat# 10600002
QA	Selleck	N/A
RNeasy kit	QIAGEN	Cat#74134
RPMI 1640	ThermoFisher Scientific	Cat# 11995-065
SB265610	Tocris Biosciences	N/A
Sodium dodecyl sulfate	Sigma	Cat# L6026
SuperScript III reverse transcriptase	Invitrogen	Cat#18080044
SYBR Green PCR master mix	ThermoFisher Scientific	Cat# 4309155
SYTOX orange	ThermoFisher Scientific	Cat#S11368
0.05% Trypsin EDTA	ThermoFisher Scientific	Cat# 25300-054
TNFα	R&D systems	Cat# DTA00D
Tris-buffered saline	Fisher-Bioreagents	Cat# BP2471-1
Triton x-100	Sigma	Cat# X100
TRIzol Reagent	ThermoFisher Scientific	Cat# 15596026
Deposited data		
Gene expression profiles of neutrophils from BALF from vehicle and virus-infected mice	GEO series database	Accession number: GSE220198
Experimental models: Organisms/strains		
C57BL/6 mice	Beijing Weitonglihua Experimental Animal Center (Beijing, China)	N/A
C57BL/6 GFP^+ mice	Beijing Weitonglihua Experimental Animal Center (Beijing, China)	N/A
Sirt2$^{fl/fl}$ mice	GemPharmatech (Nanjing, China)	N/A
Lyz-Cre mice	GemPharmatech (Nanjing, China)	N/A
human $CD34^+$ hematopoietic stem cell	Lonza	Cat# 2M-101C
Software and algorithms		
FlowJo	BD	https://www.flowjo.com/solutions/flowjo
ImageJ	Image Processing and Analysis in Java	https://imagej.nih.gov/ij/
GraphPad Prism 8	GraphPad	https://www.graphpad.com/
FlowJo software 10.8.1	Tree Star	https://www.flowjo.com/;RRID:SCR_008520

RESOURCE AVAILABILITY

Lead contact

Further information and requests for resources and reagents should be directed to and fulfilled upon reasonable request by the lead contact Guangwei Liu (liugw@bnu.edu.cn).

Materials availability

We will share any materials upon reasonable request.

Data and code availability

All data reported will be shared by the lead contact upon request. This manuscript does not report an original code. Any additional information or data required to reanalyze the data reported is available upon reasonable request to the lead contact. RNA-seq data are available on Gene Expression Omnibus (GEO accession number GSE220198).

EXPERIMENTAL MODEL AND STUDY PARTICIPANT DETAILS

Animal studies

All animal experiments were performed with the approval of the Animal Ethics Committee of Academy of Military Medical Science and Beijing Normal University (IACUC-DWZX-2017-003 and CLS-EAW-2017-002; Beijing, China). C57BL/6 (B6) and GFP$^+$ C57BL/6 mice were obtained from Beijing Weitonglihua Experimental Animal Center (Beijing, China). *Sirt2*$^{fl/fl}$ mice and *Lyz-Cre* mice were obtained from GemPharmatech (Nanjing, China). *Sirt2*$^{fl/fl}$*Lyz-Cre* mice were mated in our laboratory. All mice were bred and maintained in specific pathogen-free conditions. Sex-matched littermate mice aged 6-12 weeks were used for the experiments unless noted in the figure legends. Mice were intraperitoneally injected with a CXCR2 inhibitor (CXCR2i; SB265610, 5 mg/kg; Tocris Biosciences), AGK2 (5 mg/kg; Selleck), QA (50 μg/kg; Selleck), or FK866 (5 mg/kg; Selleck) in phosphate-buffered saline (PBS, 0.2 ml). The control group was intraperitoneally injected with PBS (0.2 ml).

Viral infection model

To establish a mouse influenza virus infection model, 50 μl of the mouse-adapted influenza virus strain A/Puerto Rico/8/34 (PR8, H1N1) at a dose of 450 TCID50 (half maximal tissue culture infectious dose) was used to intranasally infect each mouse. Mice were killed at 48 hours after virus infection, and the bronchoalveolar lavage fluid (BALF) and lungs were harvested as previously described.[33] At the indicated time points, the clinical condition of the mice was assessed by grading the severity of conjunctivitis, diarrhea, ruffled fur, and lethargy on a three-point scale. Based on the obvious differences in appearance between the treatment groups, grading was performed in a nonblinded fashion by three independent researchers. The means of the three assessments were used for grading, as described previously.[34]

Consent for publication

Written informed consent for publication was obtained from all the participants.

METHOD DETAILS

Histopathological analyses

Lung tissue was fixed in 4% paraformaldehyde and embedded in paraffin. Sections (4 μm) were mounted on positively charged glass slides. Hematoxylin and eosin (H&E) and immunohistochemical (IHC) staining with anti-mouse Ly6G (BioLegend) were performed on tissue sections as previously described.[35] Photographic analysis of H&E-stained sections and IHC sections was performed on a Zeiss Axio imager. An M1 microscope equipped with an AxioCamMR5 camera (Photometrics) with an EC plan-Neofluar 100x/0.30 numeric oil immersion lens and ZEN blue software was used (version 2012).

Neutrophil isolation and culture

At 48 hours after virus infection, the mouse BALF and lungs were harvested as described previously.[33] The lung tissue was cut into pieces and washed with RPMI 1640. Then, the lung fragments were resuspended in a 2 ml solution of 1 mg/ml collagenase XI (Sigma–Aldrich, St. Louis, MO, USA) and incubated at 37°C for 30 min. PBS supplemented with 1% FBS and 5 mM ethylenediaminetetraacetic acid (EDTA) was used to neutralize the digestion. The cells were washed twice (452 × g, 5 min), resuspended in RPMI 1640, and filtered to remove clumps. CD11b$^+$Ly6G$^+$ neutrophils were isolated from single-cell suspensions of lungs by cell sorting on a FACSAria flow cytometer (BD Biosciences, Franklin Lake, NJ, USA), as previously described.[36,37] Neutrophils were treated with FK866 (5 nM, Selleck), QA (1-10 μM, Selleck), NA (5-10 μM, Selleck), or 3-HAO (2 nM, MCE).

NET formation assay

Neutrophils were sorted from single-cell suspensions of mouse spleen or BALFs. A total of 2 × 10^5 cells was plated in 200 μl in a 96-well flat bottom plate and incubated for the indicated times. The obtained pure neutrophils were fixed with 4% paraformaldehyde for 10 mins and permeabilized with 5% Triton X-100 for 20 mins in PBS at room temperature. Neutrophils were incubated with an anti-histone H3 antibody (ab5103) for 20 mins, after which the signals were detected using Alexa Fluor® 488-conjugated anti-rabbit IgG (H + L) (Cell Signaling Technology). NETs and nucleic acids were detected by SYTOX orange (Thermo Fisher), CitH3 (ab5103) and Hoechst 33342 (Beyotime), respectively. Z-stacks (10-30 μm 40x magnification) were taken using an LSM800 instrument equipped with a 488 diode and a Plan-Apochromat 1,3 N/An Oil DIC III objective. For NET positive cell percent quantification, FIJI software and the particle analysis plugin were used. Only structures depicting NET morphology and positive Sytox Orange and CitH3 staining were selected for quantification, and intact granulocyte nuclei were excluded from the analysis. Triplicate wells of each condition were included, as described previously.[38]

Flow cytometry

The cell surface markers were analyzed via flow cytometry. The living cells were stained with buffer that included PBS containing 0.1% (weight/vol) BSA and 0.1% NaN_3 for 30 mins on ice. Flow cytometry was performed with the following antibodies from Biolegend, Abcam or R&D systems: anti-CD11b FITC (M1/70), anti-Ly6G PE (RB6-8C5), anti-TCR FITC (H57-597), anti-CD45 APC (30-F11), anti-CD44 PE (OX-50),

anti-CD62L FITC (DREG-56), anti-CD4 APC-Cy7 (RM4-5), anti-CD8α APC (EPR21769), anti-NAMPT (EPR21980), anti-SIRT2 (EP1668Y), anti-CXCR2 (242216), anti-TDO (ERP23745-311) and anti-histone H3 (citrulline R2+R8+R17; ab5103).

FACS-based intracellular staining of cytokines was performed as previously described.[39] The cells were stimulated with LPS (100 ng/ml; Sigma–Aldrich, St. Louis, MO, USA) and GolgiPlug (BD Pharmingen, Lake Franklin, NJ, USA) for 5 hours. BD Cytofix/Cytoperm and BD Perm/Wash buffer sets were used according to the manufacturer's instructions (BD Pharmingen, Lake Franklin, NJ, USA). Anti-IL-10 (ICFC) and antitumor necrosis factor α (TNFα; MP6-XT22) antibodies were obtained from Biolegend (San Diego, CA, USA). Flow cytometry data were acquired on a FACSCalibur (Becton Dickinson, CA, USA) or an Epics XL benchtop flow cytometer (Beckman Coulter, CA, USA), and the data were analyzed with FlowJo (RRID:SCR_008520; Tree Star, San Carlos, CA, USA).

Targeted metabolomics analysis

T cells were washed twice with pre-cooled PBS and extracted using pre-chilled 80% methanol (Solarbio, Beijing, China). Targeted metabolomics was performed on a liquid chromatography with tandem mass spectrometry (LC-MS/MS 8060, Shimadzu Corporation, Kyoto, Japan) equipped with an electrospray ionization source, as described previously.[40] Briefly, 5 μl cell extract was injected onto a Waters ACQUITY BEH Amide column. Separation was performed at 40°C with a flow rate of 0.4 ml/min using 10 mM ammonium acetate in water (mobile phase A) and acetonitrile (mobile phase B). The generated data was processed using Shimadzu LabSolutions Postrun Analysis (version 5.89, Shimadzu, Kyoto, Japan). The integrated peak areas of targeted metabolites were normalized to the internal standard for semi-quantification.

Immunoblot assays

Cells were lysed using RIPA buffer (Beyotime, China) with 1 mM phenylmethyl sulfonyl fluoride (Beyotime). After centrifugation, cell lysates were assessed using a BCA Protein Assay Kit (Beyotime) and boiled for denaturation with loading buffer (Beyotime). Equal amounts of protein were separated by SDS-PAGE, transferred to PVDF membranes (Millipore, USA), incubated with primary and secondary antibodies and detected with an ECL Kit (Beyotime). Immunoblotting was performed with antibodies specific for the following: QPRT (ThermoFisher), 3-HAO (Invitrogen), citH3 (Abcam), GAPDH (Abcam) and β-actin (Abcam).

Quantitative RT-PCR

RNA was extracted with a RNeasy kit (QIAGEN, Dusseldorf, Germany), and cDNA was synthesized using SuperScript III reverse transcriptase (Invitrogen, Carlsbad, CA). An ABI 7900 real-time PCR system was used for quantitative PCR, and the primer and probe sets were obtained from Applied Biosystems (Carlsbad, CA). The results were analyzed using SDS 2.1 software (Applied Biosystems). The cycling threshold value of the endogenous control gene (*Hprt*1, which encodes hypoxanthine guanine phosphoribosyl transferase) was subtracted from the cycling threshold. The expression of each target gene is presented as the fold change relative to that of the control samples, as described previously.[41]

RNA sequences

Three parallel RNA samples of BALF cells from vehicle- or virus-infected mice were extracted with TRIzol reagent and subjected to RNA sequence analysis. The read quality was assessed for each sample using FastQC, and differential expression analysis was performed with DESeq2. The RNA sequence data analysis was completed by Novogen, Beijing, China. All the data were deposited into the GEO series database under accession number GSE220198.

QPRT silenced by RNA interference

A gene-silencing lentiviral construct was generated by subcloning the gene-specific siRNA sequence into a lentiviral small interfering RNA (siRNA) expression plasmid (pMagic4.1; Sbo-bio, Shanghai, China). QPRT siRNA (5′-UAAAUCUUCCCAUCUUCAGUU-3′) and control siRNA (5′-UUCUCCGAACGUGUCACGU-3′) were synthesized (Takala Co. Ltd., Dalian, China). Lentiviruses were harvested from the culture supernatant of 293T cells (CL1032; Abgent, San Diego, CA) transfected with the siRNA vector. Sorted neutrophils from mice were stimulated for 24 hours with LPS (10 ng/ml) and infected with recombinant lentivirus. After overnight culture, the cells were restimulated for 24 hours with the virus, followed by further analysis.

NAD^+ level assay

NAD^+ levels were measured using an NAD^+/NADH assay kit (N6035, UElandy, Jiangsu, China).

ELISA

Hematopoietic stem cells-derived neutrophils were cultured and supernatants were taken and stored at -80^{0}C utilized for further analysis. A sandwich ELISA (R&D Systems) was used per the manufacturer's protocol for TNFα.

Human cell culture

Human $CD34^+$ hematopoietic stem cells (HSC; 2M-101C, Lonza)-derived neutrophils were generated as previously described.[42] In brief, HSCs were cultured in complete DMEM supplemented with 2 mM l-glutamine, 10 mM HEPES, 20 mM 2-ME, 150 U/ml streptomycin, 200 U/ml penicillin, and 10% FBS and stimulated with combinations of G-CSF (10 ng/ml; PeproTech, Rocky Hill, NJ, USA). The cultures were maintained at 37°C in a 5% CO_2 humidified atmosphere for 7 days and HSC-derived neutrophils were treated with AGK2 (5-10 μM, Selleck).

QUANTIFICATION AND STATISTICAL ANALYSIS

All the data are presented as the mean ± SD. Student's unpaired *t* test was used for the comparison of means to evaluate differences between groups. A *p* value (alpha-value) of less than 0.05 was considered to indicate statistical significance (*$p<0.05$; **$p<0.01$; ***$p<0.001$). *P*-value >0.05 was considered not significant and was denoted by ''ns''.